Article

Prolonged ^{187}Os/^{188}Os excursion implies hydrothermal influence after the Chicxulub impact in the Gulf of Mexico

Honami Sato [1,2] ✉, Akira Ishikawa [2,3], Ignacio Arenillas [4], José A. Arz [4], Vicente Gilabert [4,5], Philippe Claeys [6], Steven Goderis [6], Christopher M. Lowery[7], Sean P. S. Gulick [7,8,9] & Joanna V. Morgan [10]

The Cretaceous/Paleogene boundary asteroid impact is recorded globally as a negative ^{187}Os/^{188}Os excursion, including in sediments recovered from the IODP-ICDP drilling within the peak ring of the Chicxulub structure in the Gulf of Mexico. The reconstructed marine ^{187}Os/^{188}Os curves can be used for global age correlations on the ~10 kyr scale. However, the versatility of Os isotope clock between the proximal and distal sites remains unclear. This paper presents ^{187}Os/^{188}Os records from early Paleocene sediments deposited in the Chicxulub impact basin and Mexican sites with biochronological scales. The results for these proximal sites show a recovery timescale of ~700 kyr, which is significantly longer than that of the distal sites (~200 kyr). The interval showing the ^{187}Os/^{188}Os decline coincides with the enrichment of hydrothermally-derived Mn, implying that hydrothermal venting at the Chicxulub structure may have played a role in the marine chemistry and ecosystem of the Gulf of Mexico.

The impact event at the Cretaceous-Paleogene (K/Pg) boundary, ~66 million years ago, formed the ~200-km diameter Chicxulub impact structure on the Yucatán Platform of the Gulf of Mexico[1–4], causing a mass extinction of over 70% of the fossil species[5–7]. The decline and subsequent recovery of productivity in the marine ecosystem has been extensively studied in the K/Pg boundary sediments on a global scale[8–11]. It has been proposed that the recovery of the global marine ecosystem, measured as primary productivity, was heterogeneous[12–14]. Recent micropaleontological and geochemical studies of the impact site show a rapid recovery of both the local population and export production[15–18].

To understand post-impact changes in marine environments and ecosystems on a global scale, geochemical markers of the impact event, particularly highly siderophile element concentrations (HSEs: Os, Ir, Ru, Pt, Pd, and Re) and Os isotope ratios, can be used to accurately correlate K/Pg boundary sediments[5,19,20]. The anomalous concentration of HSEs provides a key temporal horizon that precisely links Chicxulub to K/Pg boundary sections worldwide[7,21,22]. Osmium isotope (^{187}Os/^{188}Os) records across the K/Pg boundary also constrain the time scale of the post-impact environmental recovery. Since the residence time of seawater Os (10–50 thousand years (kyr)[23,24]) is longer than the time scale of modern oceanic circulation, seawater ^{187}Os/^{188}Os values are dominated by changes in whole-ocean chemistry and relatively constant throughout the global oceans. Seawater ^{187}Os/^{188}Os

[1]Department of Earth and Planetary Sciences, Kyushu University, Fukuoka, Japan. [2]Submarine Resources Research Center, Research Institute for Marine Resources Utilization, Japan Agency for Marine-Earth Science and Technology, Yokosuka, Kanagawa, Japan. [3]Department of Earth and Planetary Sciences, Institute of Science Tokyo, Meguro-ku, Tokyo, Japan. [4]Departamento de Ciencias de la Tierra, and Instituto Universitario de Investigación en Ciencias Ambientales de Aragón, Universidad de Zaragoza, Zaragoza, Spain. [5]Departament de Dinàmica de la Terra i de l'Oceà, Facultat de Ciències de la Terra, Universitat de Barcelona, Barcelona, Spain. [6]Archaeology, Environmental Changes, and Geo-Chemistry, Vrije Universiteit Brussel, Brussels, Belgium. [7]Institute for Geophysics, Jackson School of Geosciences, University of Texas at Austin, Austin, TX, USA. [8]Deparment of Earth and Planetary Sciences, Jackson School of Geosciences, University of Texas at Austin, Austin, TX, USA. [9]Center for Planetary Systems Habitability, University of Texas at Austin, Austin, TX, USA. [10]Department of Earth Science and Engineering, Imperial College London, SW7 2AZ, London, United Kingdom. ✉e-mail: sato.honami.975@m.kyushu-u.ac.jp

ratios reflect contributions to the global ocean from weathered continental crust (^{187}Os/^{188}Os = -1.4), mantle and extraterrestrial inputs (^{187}Os/^{188}Os = -0.12–0.13)[25]. Detailed profiles of seawater ^{187}Os/^{188}Os ratios from the pelagic carbonate sections in the previous studies show similar Os isotope curves that drop sharply (^{187}Os/^{188}Os = -0.17 to 0.2) at the K/Pg boundary and then recover to their original seawater values (^{187}Os/^{188}Os = -0.4) over -200 kyr[19,20,26]. A model for the 200 kyr recovery of seawater ^{187}Os/^{188}Os in the distal sites was directly compared with age models based on biostratigraphy, magnetostratigraphy, and cyclostratigraphy, allowing independent estimates of stratigraphic time based on Os isotope analysis[20]. The development of this Os isotope based geochemical clock[20] has broad implications for paleoceanographic research, providing a tool for global correlation of pelagic carbonate sequences across the K/Pg boundary, which makes it possible to elucidate the onset of biotic crisis and subsequent recovery. However, the seawater ^{187}Os/^{188}Os curve in the Gulf of Mexico has not been reported, and correlations using the K/Pg Os isotope clock between the proximal and distal sites remain unclear.

Here, Os isotope ratios are measured in the early Paleocene limestone samples obtained from the IODP-ICDP Expedition 364 at Site M0077 in the Chicxulub impact basin in the Gulf of Mexico and early Paleocene limestone, marl, and clay samples from several sections in northeastern and southeastern Mexico (El Mulato, La Lajilla, Bochil, and Guayal sections) to reconstruct the Os isotope reference curve in the Gulf of Mexico (Figs. 1, Supplementary Note 1)[22,27,28]. Biostratigraphic correlations and calibrated ages between the Chicxulub site and the Mexican sections are calculated based on a biochronological scale relying on planktic foraminifera and astrochronological calibrations[29,30]. The obtained HSE concentrations confirm the contribution of extraterrestrial materials in proximal sediments all around the Gulf of Mexico region. For comparison, Os isotope ratios and HSE concentrations are also analyzed in suevite (polymict melt-rich impact breccia), impact melt rock, and granitic samples underlying the Paleocene limestones at Site M0077 (Supplementary Figs. 1–3).

Results

Planktic foraminiferal biochronology
Planktic foraminiferal biostratigraphy of the Paleocene white limestone for Site M0077 is updated from that published by ref. 16, which was based on P zones[31]. The planktic foraminiferal age model for Site M0077 relies on Dan zones[29]. The lowest and highest occurrence data (LOD and HOD) of key taxa occur in the correct stratigraphic order (from Dan2 to Dan4c; Supplementary Figs. 4, Supplementary Data 1). However, the LOD of *Eoglobigerina simplicissima*, which defines the base of Dan3b, could not be recognized in Site M0077, and the base of Dan3b was inferred to be at 616.23 mbsf (Supplementary Figs. 4, Supplementary Data 1).

Calibrated ages are assigned to each datum in accordance with ref. 29. The age of each sample in the Paleocene white limestone is determined by average sedimentation rates, which are constrained by the stratigraphic thickness and the calibrated time duration of the planktic foraminiferal biozones (Supplementary Figs. 4, Supplementary Data 1)[29]. Calculated sedimentation rates from each planktic foraminiferal biozone from the lower to the upper part of the white limestone are 0.667 cm kyr^{-1}, 2.6 cm kyr^{-1}, 0.125 cm kyr^{-1}, 0.669 cm kyr^{-1}, 0.256 cm kyr^{-1}, 0.068 cm kyr^{-1}, and 0.198 cm kyr^{-1} in ascending order (Supplementary Figs. 4, Supplementary Data 1). The high sedimentation rate calculated for Biozone Dan3a (2.6 cm kyr^{-1}) is anomalous, probably resulting from assuming that there is no hiatus affecting Biozone Dan3b.

Rhenium-osmium isotopes and highly siderophile elements
Age-corrected initial Os isotope ratios (^{187}Os/^{188}Os$_i$) in Site M0077 are low (^{187}Os/^{188}Os$_i$ - 0.19) in the ~3-cm-thick green-gray marlstone that transitions into the lowermost Paleocene white limestone[22] and then gradually increase in the Paleocene white limestone (Fig. 2a). ^{187}Os/^{188}Os$_i$ recover to pre-impact value (-0.4; ref. 20) at 614.32 mbsf in the lower part of Biozone Dan4c (Figs. 2a, Supplementary Data 2). In Biozone Dan4c, ^{187}Os/^{188}Os$_i$ remain constant at steady state and subsequently increase to -0.45. Based on the sedimentation rates calculated by the planktic foraminiferal age model, the depth of 614.32 mbsf corresponds to ~65.265 Ma[29], indicating that the
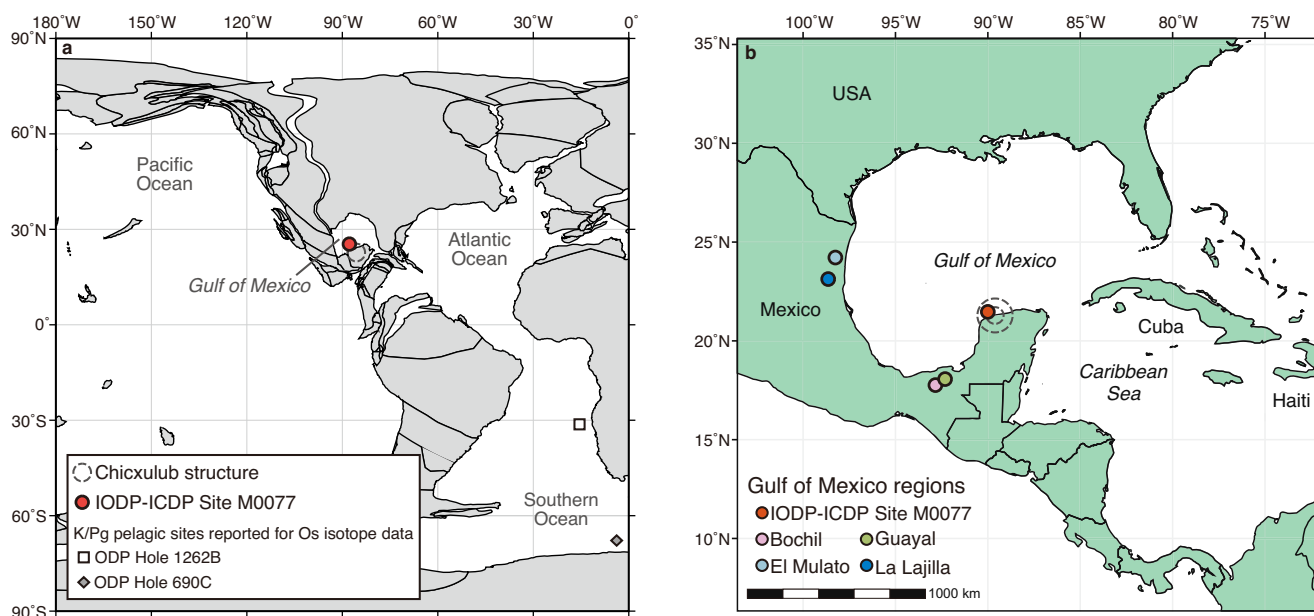

Fig. 1 | Location map. a Paleogeographic reconstruction for the K/Pg boundary (-66 Ma) showing the locations of the study site (IODP-ICDP Site M0077) within the Chicxulub impact basin and other pelagic sites reported for Os isotope profiles[20]. This map is redrawn after ref. 67 and ODSN generated at https://www.odsn.de/odsn/services/paleomap/paleomap.html. Note that this

paleoreconstruction potentially represents the placement of tectonic blocks at -66 Ma, but does not reflect sea level at the time of impact. **b** Geographic locations for the study site and sections within the Gulf of Mexico. Map modified after ref. 28.
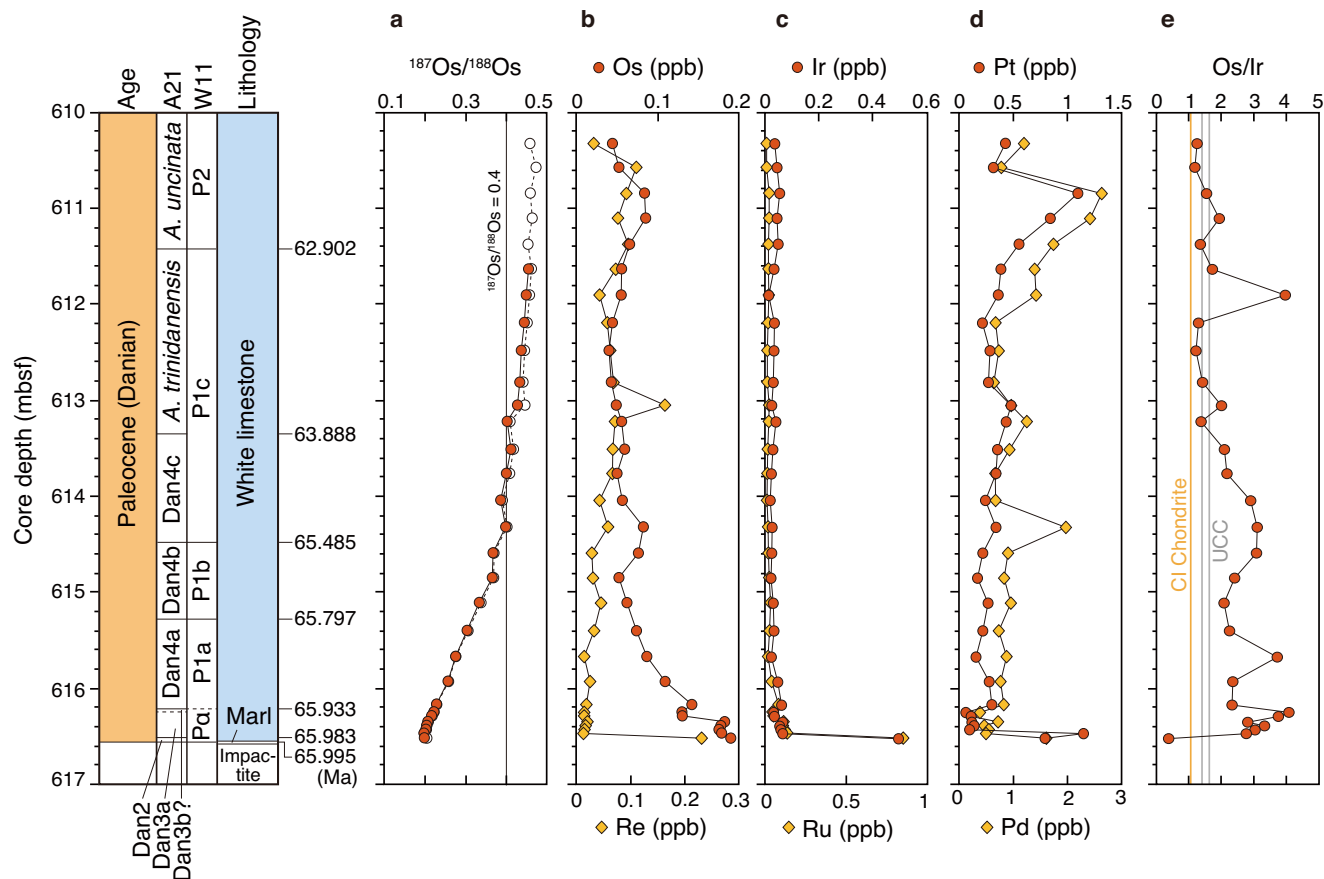
Fig. 2 | Stratigraphic profiles of $^{187}Os/^{188}Os$ ratios, HSE concentrations, and Os/Ir ratios of the Paleocene white limestone at Site M0077. a $^{187}Os/^{188}Os$ ratios represent age-corrected (red circle) and measured (white circle) isotope ratios. **b** Os and Re concentrations. **c** Ir and Ru concentrations. **d** Pt and Pd concentrations.

e Os/Ir ratios. Planktic foraminiferal zonations A21 and W11 are from ref. 29 and ref. 31, respectively. Os/Ir ratios for CI chondrite and upper continental crust (UCC) are from refs. 68–70.

recovery time of the Os isotope ratio at Site M0077 occurs more than ~700 kyr after the K/Pg impact. Measured $^{187}Os/^{188}Os$ ratios of suevite and granite underlying the Paleocene white limestone are generally high, ranging from 1.1 to 4.0 (Supplementary Figs. 5, Supplementary Data 2). In contrast, the measured $^{187}Os/^{188}Os$ ratios for the impact melt rocks display significant variations, ranging from unradiogenic values of 0.18–0.19 for the lower impact melt rocks found in the granite unit (917.18 to 917.25 mbsf) to radiogenic values of 0.9–1.5 for the upper impact melt rocks, which overlies shocked granitoid target rock of the peak ring (721.01 to 744.20 mbsf; Supplementary Figs. 1 and 5, Supplementary Data 2).

Osmium isotope ratios from marl samples in the La Lajilla section of northeastern Mexico show a minimum value ($^{187}Os/^{188}Os_i$ - 0.241) just above the K/Pg impact-induced Complex Clastic Unit (CCU)[32] and recover to ~0.3 in about 70 kyr (Figs. 3d; Supplementary Data 3). The marl samples in the El Mulato section located in northeastern Mexico show relatively high $^{187}Os/^{188}Os_i$ of ~0.320 at 1 cm above the CCU, and its lowest value about 15 cm above the CCU (Fig. 3c). Subsequently, the isotope ratios gradually increase to ~0.33 about 200 kyr after the impact. The Bochil section in southeastern Mexico shows the lowest $^{187}Os/^{188}Os_i$ values (~0.167) in the clay sample about 3 cm above the CCU and then gradually increases in the limestone and marl samples, although the Os isotopic ratios are less than 0.3 at 200 kyr after the impact (Fig. 3a). The $^{187}Os/^{188}Os_i$ ratios in the Guayal section located in southeastern Mexico show the lowest value just above the CCU (~ 0.192) in the clay sample and increase to ~0.27 in the uppermost marly limestone layer of the measured sample (~110 cm above the CCU; 80 kyr after the impact; Fig. 3b).

The Os concentrations of the Paleocene white limestone at Site M0077 gradually decrease upward throughout the limestone (Fig. 2b). The high Ir concentrations at the base of the limestone (~0.49 ppb) decrease abruptly in the lowest part of the limestone, and then remain almost constant throughout the limestone (Fig. 2b). As a result, the Os/Ir ratios of the limestones in the lower part of the study section are high compared to the ratios of upper continental crust (UCC) and CI chondrite (Fig. 2e). The concentrations of HSE show high values for Os-Ir-Ru at the base of limestone (Fig. 2), and their CI chondrite-normalized HSE patterns exhibit a relatively flat pattern (Fig. 4a)[22]. Other limestone samples between 616.48-610.33 mbsf exhibit low HSE concentrations (Fig. 2). These samples are depleted in Os-Ir-Ru and enriched in Pt-Pd-Re and characterized by Os/Ir > 1 (Figs. 2 and 4a).

The Ir and Os concentrations of the impact melt rocks are generally low, similar to the average UCC values (Supplementary Fig. 6). Only two samples, 163R3_35.5–41.0 and 163R3_47.0–48.0 from the lower impact melt rocks show slight enrichments in Os and Ir concentrations (Supplementary Fig. 6). The suevite samples are relatively similar in Os and Ir concentrations to the upper impact melt rock samples. The granite sample shows significantly lower concentrations of HSE compared to UCC (Supplementary Fig. 6).

In other Gulf of Mexico sections, Os and Ir concentrations remain high up to a few cm above the CCU (Fig. 3). The Ir concentration decrease abruptly, followed by constant low values in each section (Fig. 3). In all four sections, Os/Ir ratios show high values (Os/Ir > 1) relative to CI chondrite and UCC similar to the concentration/pattern observed at Site M0077 (Supplementary Fig. 7). The CI chondrite-normalized HSE patterns show relatively flat patterns for samples
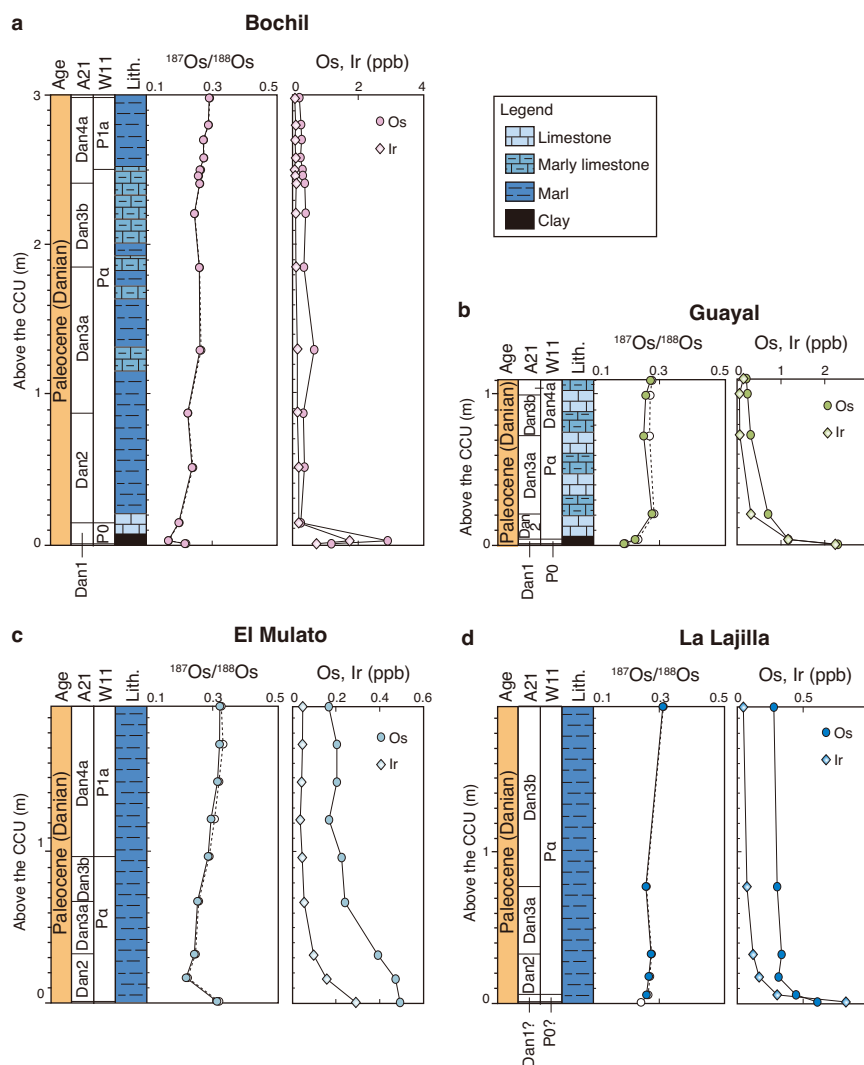
Fig. 3 | Stratigraphic sections showing age, biozones, lithology, $^{187}Os/^{188}Os$ ratios, and Os and Ir concentrations in the Mexican sections. a Bochil, **b** Guayal, **c** El Mulato, and **d** La Lajilla sections. $^{187}Os/^{188}Os$ ratios represent age corrected (colored circle) and measured (white circle) isotope ratios. Planktic foraminiferal zonations A21 and W11 are from ref. 29 and ref. 31, respectively.

immediately above the CCU, while samples at higher stratigraphic levels display coherent patterns characterized by depletion in Os-Ir-Ru relative to Pt-Pd-Re (Fig. 4b, c).

Discussion

Previously, a geochemical "clock" was proposed to determine the time elapsed since the K/Pg impact using the change from low to steady-state in the $^{187}Os/^{188}Os$ ratio[20]. This method assumes that the residence time for Os in early Paleocene seawater is ~40 kyr due to the Os one-box model after the K/Pg Chicxulub impact[20], similar to values estimated for the modern ocean (10–50 kyr)[23,24]. This makes the Os clock useful for constraining the age of sediments deposited in global oceans after the K/Pg impact. The seawater $^{187}Os/^{188}Os$ recovery from low values (~0.17) to steady state (~0.4) in ~200 kyr after the K/Pg impact relies on data obtained at ODP Hole 1262B (Walvis Ridge, South Atlantic Ocean) and ODP Hole 690 C (Maud Rise, Southern Ocean), for which the ages were based on orbital tuning and magnetostratigraphy, respectively[20]. Recently, Krahl et al. [33] revised the age of each sample from ODP Hole 1262B by interpretation derived from the astro-chronological framework and the planktic foraminifera high-resolution biostratigraphy from the well-known and also well-calibrated Zumaia section in Spain (Supplementary Data 4)[30,34]. The

age model for ODP Hole 690 C was also recalibrated against the latest paleomagnetic data (Supplementary Data 5). Although these age calibrations result in slight shifts in the $^{187}Os/^{188}Os$ curves at both pelagic sites, the length of the impact-induced Os isotope excursion remains ~200 kyr (Fig. 5a), comparable to the time scale reported by ref. 20.

The Os isotope variation of the Paleocene samples from Site M0077 within the Chicxulub impact basin is consistent with the data from both Hole 1262B and Hole 690 C showing that the ratios recover from low ($^{187}Os/^{188}Os$ ~ 0.17) to steady state values ($^{187}Os/^{188}Os$ ~ 0.4) after the K/Pg impact[19,20]. However, the recovery time for the Chicxulub impact basin occurs around ~700 kyr after the impact, much longer than ~200 kyr observed at the distal pelagic sites (Fig. 5a). Similarly, the $^{187}Os/^{188}Os_i$ recovery curves of the Bochil and El Mulato sections in the Gulf of Mexico deviate from the reference curve of the distal pelagic sites towards lower $^{187}Os/^{188}Os_i$, only reaching ~0.3 after 200 kyr (Fig. 5b).

A possible explanation for the difference between the Gulf of Mexico and pelagic $^{187}Os/^{188}Os_i$ curves is that the reduced $^{187}Os/^{188}Os$ observed for the Gulf of Mexico sediments may be due to remobilization or reworking of the K/Pg deposits enriched in chondritic components. Although the occurrence of intense sedimentary disturbances such as bioturbation or upward reworking can largely be
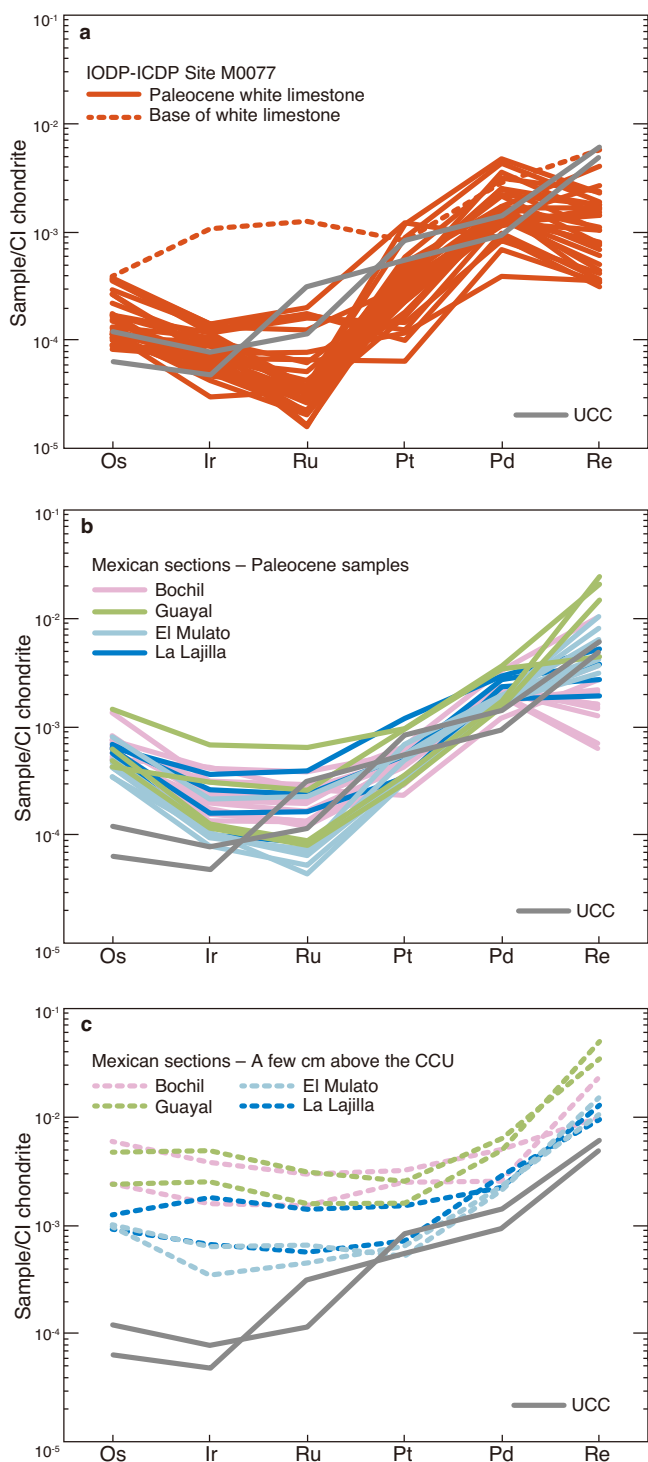
Fig. 4 | CI chondrite-normalized HSE patterns of Paleocene samples.
a Paleocene white limestones in Site M0077. The dashed line represents the sample from the base of limestone (616.52 mbsf). **b** Paleocene samples in the Mexican sections. **c** Paleocene samples from a few cm above the K/Pg impact-induced Complex Clastic Unit (CCU)[32] in the Mexican sections. The HSE patterns of upper continental crust (UCC) are also shown in comparison. HSE concentrations for CI chondrite and UCC are from refs. [68–70].

in the basal white limestone at Site M0077 (~ 0.5 ppb; ~616.52 mbsf; Figs. 2c and 4a). By contrast, the Paleocene white limestones above 616.47 mbsf show remarkably low and constant Ir concentrations (< 0.065 ppb) with the general UCC-like HSE patterns. This strongly suggests that the apparent contribution of extraterrestrial Ir ends shortly after the K/Pg impact (Figs. 2c and 4a). Similarly, sharp Ir decline after the K/Pg interval is commonly observed in the Mexican sites including the Arroyo el Mimbral[35] and other four sections studied here (Fig. 3). The basal Paleocene sediments in a few cm above the CCU and the upper sections display contrasting HSE patterns as with the Site M0077 (Fig. 4b, c). Indeed, distinct declining trends between Os and Ir abundances throughout the Paleocene sediments are broadly consistent with their contrasting residence times estimated from the modern ocean of ~40 kyr for Os and ~2 kyr for Ir[23,36] (Fig. 2 and 3), indicating that the hydrogenous component dominates the sedimentary budget. Thus, the stratigraphic variations in HSE concentrations for the Gulf of Mexico sites do not support the idea that the reduced Os isotope ratios during ~700 kyr are caused by reworking of chondritic components during Paleocene carbonate sedimentation.

From these observations, we invoke that the Paleocene sediments in the Gulf of Mexico record a continuous but unique temporal evolution of seawater Os isotopic composition after the K/Pg impact. Distinct $^{187}Os/^{188}Os$ evolutions for the global ocean and the Gulf of Mexico cannot be expected in the modern environment, since the water mass renewal rate of the Gulf of Mexico is estimated to be much faster than the Os residence time $\tau = 40$ kyr. For example, all the seawater in the Gulf of Mexico (~2.4 × 10^{15} m³) can be renewed within 3 years if the very large transports observed in the Yucatan Channel and the Straits of Florida [~27.6 Sv (1 Sv = 10^6 m³ s⁻¹); ref. 37] represent the entry and exit of the Gulf of Mexico throughflow. This in turn implies that the delayed recovery of seawater $^{187}Os/^{188}Os$ in the Gulf of Mexico could not be acquired unless the ventilation was significantly reduced shortly after the K/Pg impact.

The openness of the Gulf of Mexico to the global ocean since the Triassic-Jurassic basin opening associated with the breakup of Pangea has been discussed with paleogeographic reconstructions of the regional tectonic and depositional history[38,39]. At about 80 Ma, when sea level peaked in the Late Cretaceous[40], most reconstruction depicts the Western Interior Seaway directly connected to the Pacific. However, this connection was withdrawn by 66 Ma, leaving only the oceanic passages to the Atlantic between the Yucatán and Bahamas platforms. Recent data compilation of sedimentary sections from many industrial wells distributed throughout the Gulf of Mexico has well documented the widespread deposition of deep-water chalk and shallow marine carbonate with limited siliciclastic inputs at the end of the Cretaceous, largely due to a small number of drainage systems and circulation of ocean and shelf currents connected to the global ocean[39].

The high-energy Chicxulub impact at 66 Ma initiated earthquakes and tsunami waves, resulting in enormous redistribution of sediments into and out of the Gulf of Mexico[41,42]. For example, tsunami and mass wasting deposits recognized in the Circum-Gulf region such as Mexican and North American sites exhibit a wide range of thickness, from ~1 m to nearly 1000 m, typically containing upward fining sequences[28]. Large quantities of redistributed sediment are also documented from several sections in Cuba (< 700 m), which represent slope and basin deposits in the proto-Caribbean Sea outside the Gulf of Mexico[43]. Thus, we postulate that the impact-induced deposition generated by the tsunamigenic debris flow and platform collapse reshaped the Gulf of Mexico gateway between the Yucatán and Bahamas platforms and significantly reduced the deep-water connection to the global ocean, although there are no known estimates for the volume or thickness of deposits accumulated in the gulf entrance/exit just after the impact.

To address the delayed recovery of $^{187}Os/^{188}Os$ values in the Gulf of Mexico in this context, we carried out the Os mass balance calculation

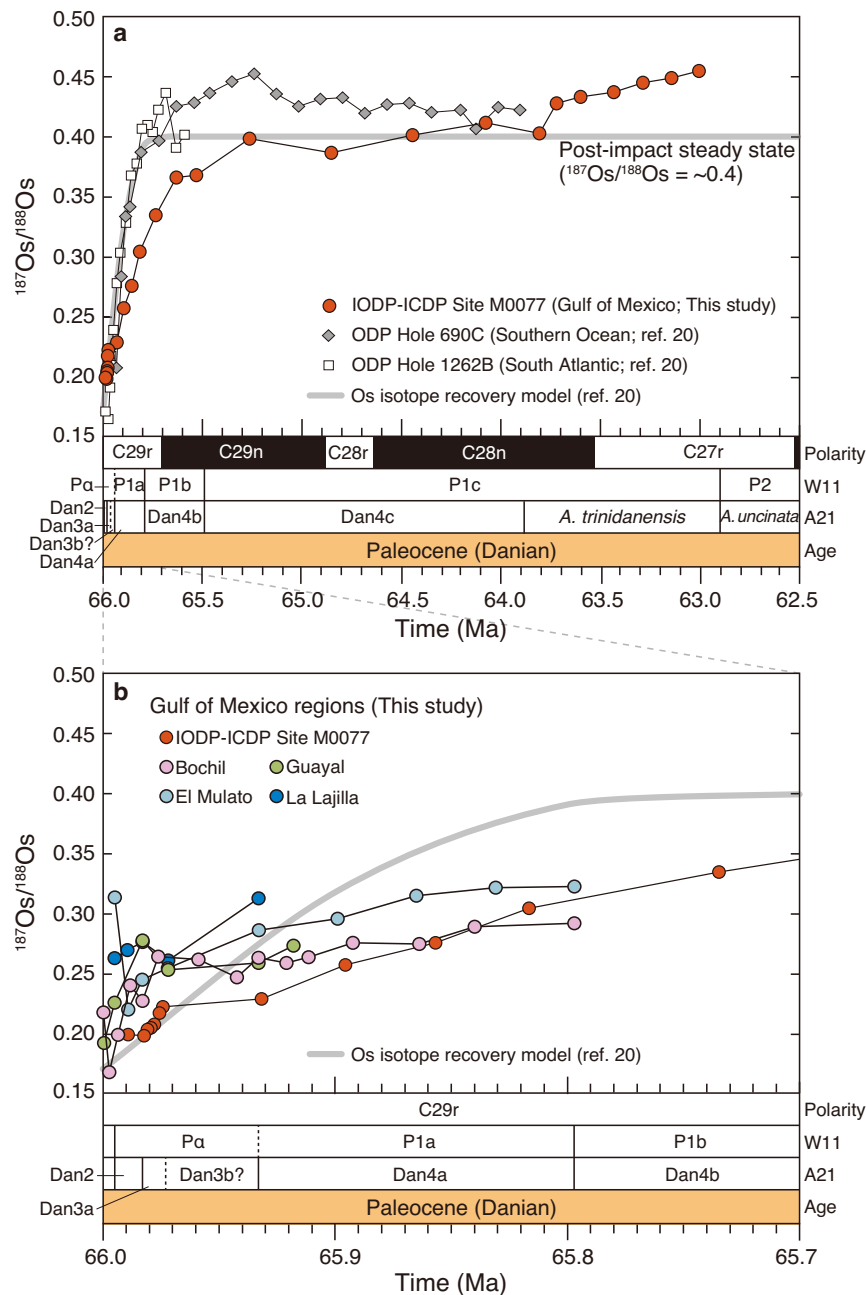ruled out for the sections studied, the possibility remains that fine meteoritic dust particles from nearby sites could be re-supplied to the Gulf of Mexico. Goderis et al. [22] identified an upward contribution of meteoritic components to post-impact sediments based on very high Ir concentration and distinctive CI chondrite-normalized HSE pattern

Fig. 5 | Comparison of $^{187}Os/^{188}Os_i$ profiles after the K/Pg impact. a $^{187}Os/^{188}Os_i$ ratios in the Chicxulub impact basin (Site M0077) and distal pelagic sites[20] for ~3.5 million years (myr) after the impact. **b** $^{187}Os/^{188}Os_i$ ratios of Paleocene (Danian) samples in the Gulf of Mexico. Gray line represents the calculated recovery model of seawater $^{187}Os/^{188}Os$ by ref. [20].

for the global ocean and the Gulf of Mexico separately using a simple box model (Supplementary Fig. 8, Supplementary Data 6). Assuming that the Gulf of Mexico is an Os pool affected by inputs of global seawater Os and unradiogenic Os sourced from chondritic impactor, the temporal evolution of seawater $^{187}Os/^{188}Os$ recorded in Site M0077 borehole is simulated if relative contributions of the two Os sources gradually change after the K/Pg asteroid impact. The model $^{187}Os/^{188}Os$ curve fitted to the Site M0077 data is reproduced under the following tuned parameters; 1) the renewal rate of water mass in the Gulf of Mexico increases from 0.015 to ~0.060 Sv between 66.001 and 63.75 Ma, and 2) meteoritic Os with unradiogenic composition is delivered to the Gulf of Mexico, decaying asymptotically from 81 mol/yr (at the K/Pg impact ~66.001 Ma) to 0 at 63.75 Ma (Supplementary Note 2, Supplementary Fig. 9, Supplementary Data 6). It should be

noted that ~0.060 Sv at 63.75 Ma is close to the maximum value for allowing the box model calculation, for given the seawater volume of the Gulf of Mexico and the Os residence time in the seawater. Actually, nearly identical $^{187}Os/^{188}Os$ between the Gulf of Mexico and the global ocean at ~65.265 Ma would support that "vigorous" flow (> ~0.060 Sv) was rapidly achieved ~700 kyr after the Chicxulub impact.

Considering that Os is known to be highly mobile during alteration and weathering processes[44,45], there are two possible mechanisms to acquire a large but continuous input of meteoritic Os with unradiogenic composition into the Gulf of Mexico: (1) through weathering of impact ejecta deposited on the nearby continents such as North America and Mexico, or (2) by venting of hydrothermal fluids reacting with the impact melt sheet underneath the Chicxulub structure[46]. Previous studies infer that a large fraction of meteoritic Os that resided

in the chondritic projectile is likely transported globally as airborne microscopic dust and impact vapor condensates that partially dissolved into seawater immediately after the impact event[22,47]. In contrast, larger fragments of melt droplets or sheets enriched in projectile components are distributed and deposited concentrically around the impact site, possibly with larger amounts downrange direction to the southwest[48,49]. Although their compositions and constituent minerals/phases remain unknown, it is possible that the incongruent weathering of these materials could have released significant and negligible amounts of unradiogenic Os and Ir, respectively. If such Os were transported with some time lag by riverine flow to the Gulf of Mexico[47], this could explain the delayed recovery of $^{187}Os/^{188}Os$ after the K/Pg impact observed in our studied sections. However, this mechanism may not be effective because the impact melt rocks enriched in HSE have rarely been observed on the continents surrounding the impact site, in contrast to their occurrence within the Chicxulub impact basin[45,48]. Furthermore, our data demonstrate that the Mexican sites distributed on the continental margin show smaller $^{187}Os/^{188}Os$ excursions than that of Site M0077, located in the impact basin (Fig. 5b). In other words, the largest $^{187}Os/^{188}Os$ excursion for Site M0077 among the study sites likely indicates that the crater hydrothermal mechanism is the dominant process for introducing the unradiogenic Os into the Gulf of Mexico seawater. Indeed, contemporaneous limestones from Site M0077 show excess concentrations of Mn, P, and Pb during reduced $^{187}Os/^{188}Os$ ratios[16,27,46]. Kring et al.[46] suggest that Mn enrichment in post-impact limestone sediments overlying suevite may be due to hydrothermal venting after the impact at Site M0077. Therefore, delayed recovery of seawater $^{187}Os/^{188}Os$ in the Gulf of Mexico suggest that it is influenced by a long-term supply of hydrothermal fluids activated in the Chicxulub structure after the impact event, as discussed below.

The Chicxulub impact uplifted crustal rocks from a depth of 8–10 km and produced a melt sheet of 10^4–10^5 km³ (refs. 50,51). Such a large impact event generates long-term heat sources that include shock-deposited heat, a large melt sheet, and a central uplift. The impact event created a porous and permeable structure in the Chicxulub impact structure that was an ideal host for the hydrothermal fluid system. Numerical simulations of the hydrothermal activity in the Chicxulub structure indicate that the system extended to a depth of 5–6 km and its lifetime (i.e., the time required for the system to cool below 90 °C within 1 km of the surface) ranges from 1.5 to 2.3 million years[52]. Mineralogical observations over almost the entire length of Site M0077 drill core support an extended duration thermal evolution model. The volume of area is estimated at ~1.4 × 10⁵ km³ (ref. 46).

The hydrothermal activity at Chicxulub structure could play a significant role in the observed $^{187}Os/^{188}Os$ variations in the Gulf of Mexico seawater. This is inferred from the recent study demonstrating that the 5.8 m thick early Paleocene limestones in the M0077 core contain significant amounts of Mn released from post-impact hydrothermal plumes into the Gulf of Mexico seawater (Fig. 6b)[46]. Although early Paleocene limestones from Site M0077 do not show a significant change in color (Supplementary Fig. 2), a strong positive correlation between Os/Al and Mn/Al ($R^2 = 0.90$) was observed for our data during the delayed recovery of $^{187}Os/^{188}Os$ values (614.32 to 616.57 mbsf). Other geochemical proxies for hydrothermal activity such as the P and Pb enrichments[53,54] are also observed in the interval with unradiogenic $^{187}Os/^{188}Os$ (Fig. 6). This covariation strongly suggests that together with Mn, P, and Pb, the hydrothermal plumes supplied unradiogenic Os into the Gulf of Mexico for at least ~700 kyr after the Chicxulub impact, based on our calibrated age. Similar Mn, P, and Pb enrichments occurs in post-impact hydrothermal sediments of another drill core within the Chicxulub structure (ICDP Yaxcopoil-1)[53]. In the Sudbury structure, Mn, P, and Pb enrichments are also observed in the Onaping formation[55].

At mid-ocean ridge vents, Mn oxidizes more slowly than other dissolved elements in hydrothermal plumes, and Mn oxide particles can be transported for several hundreds of km, before precipitating out of suspension to form sediments[53,56]. Studies of present and past marine sediments suggest that Os dissolved in seawater is adsorbed onto Mn (oxyhydr) oxide particles, preserving the seawater $^{187}Os/^{188}Os$
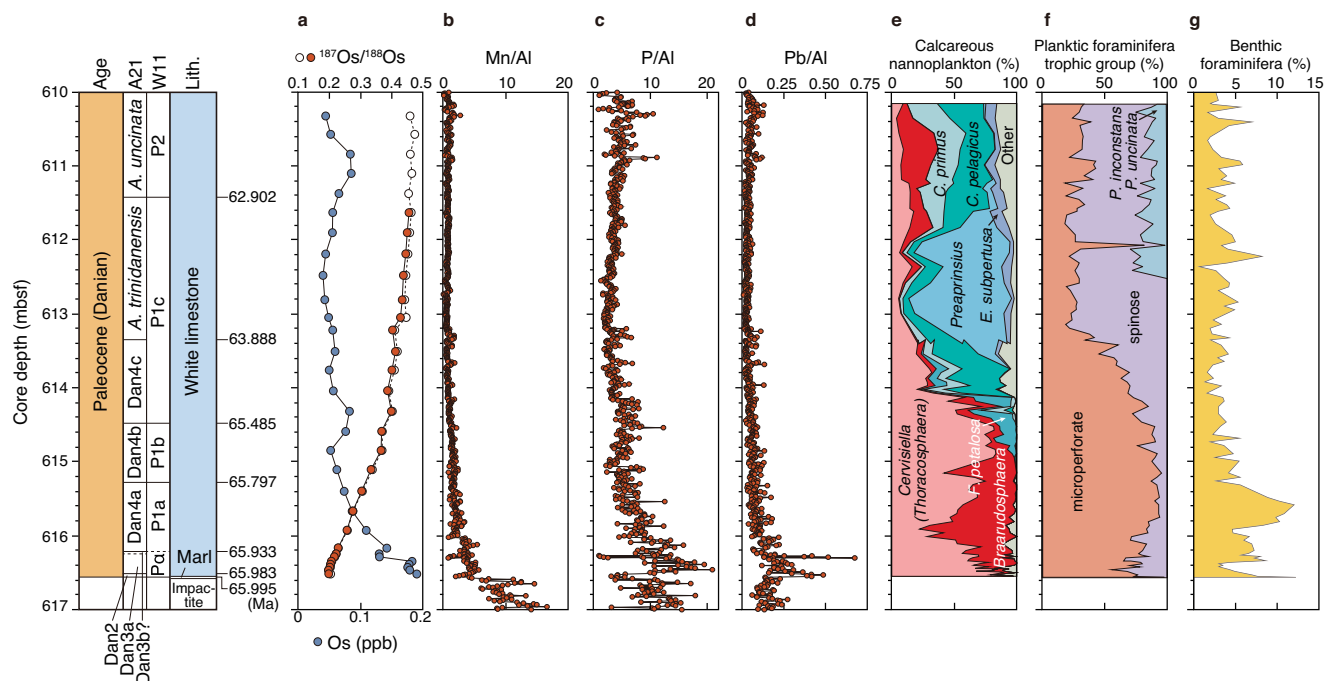

Fig. 6 | Osmium isotope profile and paleoenvironmental change after the impact event. a Age-corrected (red circle) and measured (white circle) $^{187}Os/^{188}Os$ ratio and Os concentration at Site M0077. **b**, **c** and **d** are XRF core scan data reported by ref. 16. Data of **e**, **f**, and **g** are from ref. 62 and ref. 16, respectively. **e** Relative abundance plots for nannoplankton taxa. **f** Relative abundance of planktic foraminiferal trophic groups. **g** The percentage of benthic foraminifera relative to all foraminifera.

in the sediments[25,57–59]. Although mantle-derived unradiogenic Os is released from hydrothermal vents at mid-ocean ridge settings, it is difficult to presume the Os isotope ratios in the Chicxulub hydrothermal plumes. If the amount of meteoritic material introduced into the Chicxulub impact structure was low due to the assumed steeply-inclined trajectory of the impactor[60,61], highly radiogenic Os derived from the pre-impact lithologies (continental granites) may have been dominated in hydrothermal fluids.

Feignon et al. [45] reported the $^{187}Os/^{188}Os$ values and HSE compositions of suevites and impact melt rocks as well as pre-impact lithologies recovered from Site M0077 on the peak ring. Since the majority of samples display low Ir contents (< 40 ppt) with HSE patterns similar to those for typical crustal compositions (e.g., UCC), they concluded that any meteoritic components within the crater are highly diluted. However, two impact melt rocks exhibit significant enrichments of Ir (250–324 ppt) and Os (125–344 ppt), which are likely attributed to meteoritic contamination. The most striking feature of the depth profile of M0077 drill core is that the $^{187}Os/^{188}Os$ ratios of the granitic basement and impact melt rocks in the lower unit (750-1250 mbsf) are consistently low ($^{187}Os/^{188}Os$ < 0.2), indicative of the post-impact hydrothermal overprint on an extensive part of the basement (Supplementary Fig. 5). This is supported by the fact that the least altered amphibolite (80R2_61–63.5) and granite (95R1_91.0–93.0) preserve highly radiogenic $^{187}Os/^{188}Os$ ratios of 2.47 and 4.02, respectively. Assuming that these two samples represent pre-impact lithologies, mixing calculation traces the contamination of the meteoritic component. The majority of data from the basement broadly follows mixing areas between radiogenic amphibolite-granite and chondrite on a diagram of $^{187}Os/^{188}Os$ versus Os concentration, even though the data for Os/Ir ratios versus $^{187}Os/^{188}Os$ tend to deviate toward higher Os/Ir ratios from the mixing areas (Supplementary Fig. 10). These deviations can be attributed to the selective hydrothermal remobilization of Os but not for Ir. Some contributions from mafic target rock cannot be ruled out due to the occurrence of Os-rich dolerite dykes in the depth interval (854.6 mbsf: 140R2_5–8). Nevertheless, the data strongly suggest that hydrothermal fluids within the Chicxulub structure mobilized unradiogenic Os, which could then affect the seawater $^{187}Os/^{188}Os$ ratios of Gulf of Mexico seawater via prolonged hydrothermal venting.

If the above scenario is plausible, temporal relationship between hydrothermal supply of nutrients and marine ecosystem change should be examined carefully. Detailed analyzes of a record of calcareous nannoplankton and planktic foraminifera from Site M0077 reveal that life in the impact basin reappeared soon after the impact, and that a high-productivity ecosystem is established after only ~30 kyr[15]. Their post-extinction assemblages are dominated by calcareous dinoflagellate cysts (*Cervisiella* spp.), *Braarudosphaera* spp., and microperforate foraminifera, all of which are adapted to high-nutrient (eutrophic) environments (Fig. 6e, f)[62]. Furthermore, the abundance of benthic foraminifera relative to planktic foraminifera, which can be regarded as an indicator of organic matter fluxes from the surface ocean to the deep seafloor, increased sharply in Biozone Dan4a (Fig. 6g)[16]. It has been presumed that these recovery patterns are likely driven by ecological rather than environment processes[16,62].

Interestingly, the time scale for complete recovery from the impact induced Os isotope excursion coincides with a transition in the marine ecosystem from eutrophic to oligotrophic conditions (Fig. 6e, f). Turnovers in the calcareous nannoplankton and planktic foraminiferal assemblages are marked in Biozone Dan4c, which coincide with the lower part of Biozone P1c (Fig. 6e, f). In this stratigraphic interval of 65.485–63.888 Ma, calibrated by biochronological scale (Supplementary Data 1), seawater $^{187}Os/^{188}Os_i$ ratios in the Gulf of Mexico become identical to those of the steady-state recorded in the pelagic sites (~0.4)[20]. Also, at this interval, Mn, P, and Pb concentrations decrease to background levels inferred from overlying middle

Paleocene sediments (Fig. 6). Indeed, the declining pattern of P concentration in early Paleocene limestone at Site M0077 at 614 mbsf and further at 613.2 mbsf coincides with major assemblage changes in the calcareous nannoplankton and planktic foraminifera trophic group (Fig. 6c, e, f). While this timing may be coincidental, these covariations suggest that the hydrothermal activity in the impact basin led to large-scale shifts in the dominant nannoplankton and planktic foraminiferal trophic groups, and that the hydrothermal supply of phosphorus, a limiting nutrient in primary productivity facilitated the early recovery of diverse life, as speculated by ref. 17.

Our study infers that there are some intimate relationships between the impact-induced hydrothermal activity and the biosphere recovery within the Chicxulub impact basin. However, in order to test the scenario that hydrothermal supply of nutrients and energy was a key driver for changes in the biota of the marine surface environment, it is necessary to clarify how these nutrients were supplied by the hydrothermal system and entered the euphotic zone to drive enhanced primary production. Because there are no large-scale hydrothermal systems in the oceans today comparable to that formed by the Chicxulub impact, sedimentary records from variable sites in nearby oceans are critical to examining the extents of hydrothermal effects on the marine surface environment. For example, there is the problem of why similar trends in export productivity (e.g., Ba/Ti ratio) are observed in the Caribbean Sea[63], far from the hydrothermal system, which cannot be explained if we assume that the supply of nutrients from the hydrothermal system was limited to the Gulf of Mexico. Thus, further research on Os isotope and other geochemical profiles in different sites such as the Caribbean Sea and the Pacific Ocean are clearly required to confirm the versatility of the Os isotope clocks and to reconstruct the recovery patterns of the marine ecosystem.

Methods

Planktic foraminiferal analyzes
The age models for Site M0077 and Mexican sections (El Mulato, La Lajilla, Bochil, and Guayal) are based on planktic foraminifera high-resolution biostratigraphy (see refs. 16,28,29; and references herein). The studied rock samples were disaggregated using two techniques; 1) using a H_2O_2 solution for 6 to 24 h (to disaggregate marl and clay samples), and 2) using a solution with 80% acetic acid for 4 to 6 h (to disaggregate very lithified marly limestone and limestone samples). The residual fractions were then washed through a 63 µm sieve and dried at 50°C.

All correlations and ages were obtained following the same taxonomic and biostratigraphic criterion (Supplementary Data 1 and 3). The planktic foraminiferal biochronological scale used was magnetochronologically calibrated by refs. 29,64, and astrochronologically by ref. 30. This scale is based on the Dan biozonation of ref. 29, which used the following key-biohorizons: HOD of *Abathomphalus mayaroensis* (= K/Pg mass extinction event; 66.001 Ma; base of Dan1), LOD of *Parvularugoglobigerina longiapertura* (65.995 Ma; base of Dan2), LOD of *Parvularugoglobigerina eugubina* (65.983 Ma; base of Dan3a), LOD of *Eoglobigerina simplicissima* (65.973 Ma; base of Dan3b), LOD of *Parasubbotina pseudobulloides* (65.933 Ma; base of Dan4a), LOD of *Subbotina triloculinoides* (65.797 Ma; base of Dan4b), and LOD of *Globanomalina compressa* (65.485 Ma; base of Dan4c). The biostratigraphic study of Site M0077 also includes the following key-biohorizons: LOD of *Acarinina trinidadensis* (base of homonym biozone), and LOD of *Acarinina uncinata* (base of homonym biozone), magnetochronologically calibrated at 63.888 and 62.902 Ma by ref. 64.

Re-Os isotope and highly siderophile element analyzes
Rhenium-osmium (Re-Os) isotope compositions and highly siderophile element (HSE: Os, Ir, Ru, Pt, Pd, and Re) concentrations for

23 samples of Paleocene limestone and 16 samples (with 1 replicate) of suevite, impact melt rock, and granite within the Chicxulub impact basin, and 36 Paleocene samples from other K/Pg sites around the Gulf of Mexico (Bochil, Guayal, El Mulato, and La Lajilla sections) were determined by isotope dilution mass spectrometry (ID-MS) after quartz glass tube digestion. The methods used for sample digestion, chemical purification, and mass spectrometry are based on procedures outlined in refs. 59,65. Powdered samples (-0.25–0.5 g) and spike solutions enriched in ^{185}Re and mixed ^{190}Os-^{191}Ir-^{99}Ru-^{196}Pt-^{105}Pd were transferred into a quartz glass tube. After adding 3–4 mL of inverse aqua regia, each quartz glass tube was frozen in dry ice, sealed with an oxygen-propane torch, and placed in an oven at 240 °C for 72 h. Subsequently, 1–3 mL of 38% hydrofluoric acid (HF) was added to the residual solids after Os extraction for desilicification.

Isotope ratio measurements of HSE were conducted using two types of mass spectrometers. Osmium concentrations and isotopic compositions were measured by negative thermal ionization mass spectrometry (N-TIMS; Triton Plus, Thermo Fisher Scientific) at JAM-STEC, Japan. Osmium purified after CCl_4 solvent extraction and microdistillation[66] was loaded in HBr on baked 99.997% Alfa Aesar Pt wire and covered with a NaOH-Ba(OH)$_2$ activator solution. The average total procedural blank for Os was 0.32 ± 0.46 pg ($n = 9$, 1 SD) with a ^{187}Os/^{188}Os ratio of 0.152 ± 0.015. Blank corrections were applied to all analyzes, which relies on the blank associated with each batch of digestion rather than using a long-term average. The uncertainties for ^{187}Re/^{188}Os and ^{187}Os/^{188}Os were estimated by error propagation of the blank uncertainties. Blank contributions for the measured Os concentrations and ^{187}Os/^{188}Os ratios of the samples from the Paleocene limestone in Site M007 were mostly insignificant: less than 1.4% and 0.9%, respectively. The blank contributions for the suevite, impact melt rocks and granite samples were variable depending on their Os concentrations (0.2–4.7% for Os and 0.03–4.8% for ^{187}Os/^{188}Os). The blank contributions for the measured Os concentrations and ^{187}Os/^{188}Os ratios for the samples from other Gulf of Mexico regions were less than 0.7% and 0.3%, respectively.

Purification of Ir, Pt, Ru, Pd, and Re was accomplished in three steps: (1) anion exchange chromatography; (2) cation exchange chromatography; and (3) solvent extraction using N-benzoyl-N-phenylhydroxylamine (BPHA). HSE concentrations were measured by high-resolution ICP-MS (HR-ICP-MS; Element XR, Thermo Fisher Scientific) housed in the University of Tokyo at Komaba. For sample introduction, a combination of 100 μ/min PFA self-aspirating nebulizer and dual cyclonic/Scott double-pass spraychamber was used during all measurements, and oxide level (HfO$^+$/Hf) was set to 1%. Sample and standard solutions were interspersed throughout the analytical sessions to monitor and correct for instrumental fractionation. The monitored masses of analyzes and interferences are ^{89}Y, ^{90}Zr, ^{95}Mo, ^{97}Mo, ^{99}Ru, ^{100}Ru, ^{101}Ru, ^{105}Pd, ^{106}Pd, ^{108}Pd, ^{111}Cd, ^{178}Hf, ^{185}Re, ^{187}Re, ^{191}Ir, ^{193}Ir, ^{194}Pt, ^{195}Pt, ^{196}Pt, and ^{202}Hg. Although all raw signal intensities of samples were mathematically corrected for the measured isobaric oxide interferences, contributions of interferences to analyte signals are mostly insignificant (< 0.1%). The average total procedural blanks for the analyzed elements are 2.3 ± 1.7 pg for Ir, 1.4 ± 0.1 pg for Ru, 22 ± 7 pg for Pt, 4.0 ± 2.6 pg for Pd, and 1.9 ± 0.8 pg for Re ($n = 9$, 1 SD). As in the case of Os, all analyzes were blank-corrected. Blank contributions to samples from Site M0077 for Ir, Ru, Pt, Pd, and Re were < 37%, < 21%, < 22%, < 2.2%, and < 20%, respectively, except for granite sample 95R1_91.0-93.0 (42% for Ir, 22% for Pt, 52% for Pd, and 0.4% for Re). The blank contributions to samples from other Gulf of Mexico regions for Ir, Ru, Pt, Pd, and Re were < 3.0%, <12%, < 32%, <1.1%, and < 29%, respectively. The uncertainties on each sample were estimated by error propagation of the analytical uncertainties during ICP-MS measurement (2SE) and blank correction. The accuracy of the analytical methods was evaluated by measuring basaltic (BIR-1a) and sedimentary limestone (JLs-1) reference materials (Supplementary Data 2).

Nine replicates of BIR-1a display good reproducibility (0.3% RSD for ^{187}Os/^{188}Os, 12% RSD for Os, 12% RSD for Ir, 4.2% RSD for Ru, 5.4% RSD for Pt, 4.5% RSD for Pd, and 1.3% RSD for Re in the -0.5 g powdered samples; $n = 9$) and are in good agreement with data for larger powdered samples (-1 g; ref. 65). JLs-1 also displays good reproducibility for ^{187}Os/^{188}Os (0.5%) and Os (0.3%) and Re (1.5%) concentrations, whereas other HSE concentrations show larger variability (33% RSD for Ir, 53% RSD for Ru, 64% RSD for Pt, and 31% RSD for Pd in the -0.5 g powdered samples; $n = 4$) due to their very low HSE concentrations.

Data availability
All data generated in this study are provided in the Supplementary Information and Supplementary Data.

References

1. Hildebrand, A. R. et al. Chicxulub crater: a possible Cretaceous/Tertiary boundary impact crater on the Yucatán Peninsula. Mexico. *Geology* **19**, 867–871 (1991).
2. Swisher, C. C. et al. Coeval ^{40}Ar/^{39}Ar ages of 65.0 million years ago from Chicxulub crater melt rock and Cretaceous-Tertiary boundary tektites. *Science* **257**, 954–958 (1992).
3. Gulick, S. P. S. et al. Importance of pre-impact crustal structure for the asymmetry of the Chicxulub impact crater. *Nat. Geosci.* **1**, 131–135 (2008).
4. Renne, P. R. et al. Time scales of critical events around the Cretaceous-Paleogene boundary. *Science* **339**, 684–687 (2013).
5. Alvarez, L. W., Alvarez, W., Asaro, F. & Michel, H. V. Extraterrestrial cause of the Cretaceous-Tertiary extinction. *Science* **208**, 1095–1108 (1980).
6. Jablonski, D. & Chaloner, W. G. Extinctions in the fossil record [and discussion]. *Philos. Trans.: Biol. Sci.* **344**, 11–17 (1994).
7. Schulte, P. et al. The Chicxulub asteroid impact and mass extinction at the Cretaceous-Paleogene boundary. *Science* **327**, 1214–1218 (2010).
8. Zachos, J. C., Arthur, M. A. & Dean, W. E. Geochemical evidence for suppression of pelagic marine productivity at the Cretaceous/Tertiary boundary. *Nature* **337**, 61–64 (1989).
9. D'Hondt, S., Donaghay, P., Zachos, J. C., Luttenberg, D. & Lindinger, M. Organic carbon fluxes and ecological recovery from the Cretaceous-Tertiary mass extinction. *Science* **282**, 276–279 (1998).
10. Coxall, H. K., D'Hondt, S. & Zachos, J. C. Pelagic evolution and environmental recovery after the Cretaceous-Paleogene mass extinction. *Geology* **34**, 297–300 (2006).
11. Birch, H., Schmidt, D. N., Coxall, H. K., Kroon, D. & Ridgwell, A. Ecosystem function after the K/Pg extinction: decoupling of marine carbon pump and diversity. *Proc. R. Soc. B: Biol. Sci.* **288**, 20210863 (2021).
12. Alegret, L., Molina, E. & Thomas, E. Benthic foraminifera at the Cretaceous-Tertiary boundary around the Gulf of Mexico. *Geology* **29**, 891–894 (2001).
13. Alegret, L. & Thomas, E. Cretaceous/Paleogene boundary bathyal paleo-environments in the central North Pacific (DSDP Site 465), the Northwestern Atlantic (ODP Site 1049), the Gulf of Mexico and the Tethys: The benthic foraminiferal record. Palaeogeogr. *Palaeoclimatol. Palaeoecol.* **224**, 53–82 (2005).
14. Hull, P. M. & Norris, R. D. Diverse patterns of ocean export productivity change across the Cretaceous-Paleogene boundary: New insights from biogenic barium. *Paleoceanogr* **26**, PA3205 (2011).
15. Lowery, C. M. et al. Rapid recovery of life at ground zero of the end-Cretaceous mass extinction. *Nature* **558**, 288–291 (2018).
16. Lowery, C. M. et al. Early Paleocene paleoceanography and export productivity in the Chicxulub crater. *Paleoceanogr. Paleoclimatol.* **36**, e2021PA004241 (2021).
17. Bralower, T. J. et al. The habitat of the nascent Chicxulub crater. *AGU Adv.* **1**, e2020AV000208 (2020).

18. Schaefer, B. et al. Microbial life in the nascent Chicxulub crater. *Geology* **48**, 328–332 (2020).

19. Ravizza, G. & Peucker-Ehrenbrink, B. Chemostratigraphic evidence of Deccan volcanism from the marine osmium isotope record. *Science* **302**, 1392–1395 (2003).

20. Ravizza, G. & VonderHaar, D. A geochemical clock in earliest Paleogene pelagic carbonates based on the impact-induced Os isotope excursion at the Cretaceous-Paleogene boundary. *Paleoceanogr* **27**, PA3219 (2012).

21. Goderis, S. et al. Reevaluation of siderophile element abundances and ratios across the Cretaceous-Paleogene (K-Pg) boundary: implications for the nature of the projectile. *Geochim. Cosmochim. Acta* **120**, 417–446 (2013).

22. Goderis, S. et al. Globally distributed iridium layer preserved within the Chicxulub impact structure. *Sci. Adv.* **7**, eabe3647 (2021).

23. Levasseur, S., Birck, J.-L. & Allegre, C. J. The osmium riverine flux and the oceanic mass balance of osmium. *Earth Planet. Sci. Lett.* **174**, 7–23 (1999).

24. Oxburgh, R. Residence time of osmium in the oceans. *Geochem. Geophys. Geosyst* **2**, 2000GC000104 (2001).

25. Peucker-Ehrenbrink, B. & Ravizza, G. The marine osmium isotope record. *Terra Nova* **12**, 205–-219 (2000).

26. Robinson, N., Ravizza, G., Coccioni, R., Peucker-Ehrenbrink, B. & Norris, R. A high-resolution marine $^{187}Os/^{188}Os$ record for the late Maastrichtian: distinguishing the chemical fingerprints of Deccan volcanism and the KP impact event. *Earth Planet. Sci. Lett.* **281**, 159–168 (2009).

27. Morgan, J. V. et al. *Proceedings of the International Ocean Discovery Program, Volume 364: Drilling the K-Pg impact crater* (International Ocean Discovery Program, College Station, TX, 2017).

28. Arz, J. A. et al. No evidence of multiple impact scenario across the Cretaceous/Paleogene boundary based on planktic foraminiferal biochronology. *Geol. Soc. Am. Spec. Pap.* **557**, 415–448 (2022).

29. Arenillas, I., Gilabert, V. & Arz, J. A. New biochronological scales of planktic foraminifera for the early Danian based on high-resolution biostratigraphy. *Geosciences* **11**, 479 (2021).

30. Gilabert, V., Batenburg, S. J., Arenillas, I. & Arz, J. A. Contribution of orbital forcing and Deccan volcanism to global climatic and biotic changes across the Cretaceous-Paleogene boundary at Zumaia, Spain. *Geology* **50**, 21–25 (2022).

31. Wade, B. S., Pearson, P. N., Berggren, W. A. & Pälike, H. Review and revision of Cenozoic tropical planktonic foraminiferal biostratigraphy and calibration to the geomagnetic polarity and astronomical time scale. *Earth-Sci. Rev.* **104**, 111–142 (2011).

32. Arenillas, I. et al. Chicxulub impact event is Cretaceous/Paleogene boundary in age: New micropaleontological evidence. *Earth Planet. Sci. Lett.* **249**, 241–257 (2006).

33. Krahl, G. et al. Impact of early Danian environmental perturbations on mid-latitude planktic foraminiferal assemblages from the ODP Site 1262 (South Atlantic Ocean). *Newslett. Stratigr.* **56**, 377–403 (2023).

34. Dinarès-Turell, J., Westerhold, T., Pujalte, V., Röhl, U. & Kroon, D. Astronomical calibration of the Danian stage (Early Paleocene) revisited: settling chronologies of sedimentary records across the Atlantic and Pacific Oceans. *Earth Planet. Sci. Lett.* **405**, 119–131 (2014).

35. Smit, J. et al. Tektite-bearing, deep-water clastic unit at the Cretaceous-Tertiary boundary in northeastern Mexico. *Geology* **20**, 99–103 (1992).

36. Lee, C. T. A., Wasserburg, G. J. & Kyte, F. T. Platinum-group elements (PGE) and rhenium in marine sediments across the Cretaceous–Tertiary boundary: constraints on Re-PGE transport in the marine environment. *Geochim. Cosmochim. Acta* **67**, 655–670 (2003).

37. Candela, J. et al. The flow through the Gulf of Mexico. *J. Phys. Oceanogr.* **49**, 1381–1401 (2019).

38. Escalona, A., Ahmad, S. S. & Watson, L. Late Cretaceous-Pliocene paleogeography of the circum-Caribbean region based on quantitative plate reconstructions and georeferenced databases. In *South America-Caribbean-Central Atlantic plate boundary: Tectonic evolution, basin architecture, and petroleum systems: AAPG Memoir*, 123, 513–538 (The American Association of Petroleum Geologists, 2021).

39. Snedden, J. W., Lowery, C. M. & Lawton, T. F. The end of the Cretaceous: depositional palaeogeographical reconstruction of the Gulf of Mexico and adjacent areas just prior to the Chicxulub impact. *Geol. Soc., Lond., Spec. Pub.* **545**, SP545 (2024).

40. Marcilly, C. M., Torsvik, T. H. & Conrad, C. P. Global Phanerozoic sea levels from paleogeographic flooding maps. *Gondwana Res* **110**, 128–142 (2022).

41. Bralower, T. J., Paull, C. K. & Leckie, R. M. The Cretaceous-Tertiary boundary cocktail: Chicxulub impact triggers margin collapse and extensive sediment gravity flows. *Geology* **26**, 331–334 (1998).

42. Sanford, J. C., Snedden, J. W. & Gulick, S. P. S. The Cretaceous-Paleogene boundary deposit in the Gulf of Mexico: large-scale oceanic basin response to the Chicxulub impact. *J. Geophys. Res.: Solid Earth* **121**, 1240–1261 (2016).

43. Scott, E., Denne, R., Kaiser, J. & Eickhoff, D. Impact on sedimentation into the north-central deepwater Gulf of Mexico as a result of the Chicxulub event. *Gulf Coast Assoc. Geol. Sci. J.* **3**, 41–50 (2014).

44. Wimpenny, J. et al. Rhenium and osmium isotope and elemental behaviour accompanying laterite formation in the Deccan region of India. *Earth Planet. Sci. Lett.* **261**, 239–258 (2007).

45. Feignon, J.-G. et al. Search for a meteoritic component within the impact melt rocks of the Chicxulub impact structure peak ring, Mexico. *Geochim. Cosmochim. Acta* **323**, 74–101 (2022).

46. Kring, D. A. et al. Probing the hydrothermal system of the Chicxulub impact crater. *Sci. Adv.* **6**, eaaz3053 (2020).

47. Paquay, F. S., Ravizza, G. E., Dalai, T. K. & Peucker-Ehrenbrink, B. Determining chondritic impactor size from the marine osmium isotope record. *Science* **320**, 214–218 (2008).

48. Koeberl, C. et al. Evidence for a meteoritic component in impact melt rock from the Chicxulub structure. *Geochim. Cosmochim. Acta* **58**, 1679–1684 (1994).

49. Artemieva, N. & Morgan, J. Global K–Pg layer deposited from a dust cloud. *Geophys. Res. Lett.* **47**, 1–8 (2020).

50. Morgan, J. V. et al. The formation of peak rings in large impact craters. *Science* **354**, 878–882 (2016).

51. Kring, D. A. The dimensions of the Chicxulub impact crater and impact melt sheet. *J. Geophys. Res.: Planets* **100**, 16979–16986 (1995).

52. Abramov, O. & Kring, D. A. Numerical modeling of impact-induced hydrothermal activity at the Chicxulub crater. *Meteorit. Planet. Sci.* **42**, 93–112 (2007).

53. Rowe, A. J., Wilkinson, J. J., Coles, B. J. & Morgan, J. V. Chicxulub: testing for post-impact hydrothermal input into the Tertiary ocean. *Meteorit. Planet. Sci.* **39**, 1223–1231 (2004).

54. Pirajno, F. Hydrothermal processes associated with meteorite impacts. In *Hydrothermal Processes and Mineral Systems*, 1097–1130 (Springer Netherlands, 2009).

55. Desborough, G. A. & Larson, R. R. Nickel-bearing iron sulfides in the onaping formation, Sudbury Basin, Ontario. *Economic Geol.* **65**, 728–730 (1970).

56. Mottl, M. J. et al. Manganese and methane in hydrothermal plumes along the East Pacific Rise, 8°40' to 11°50'N. *Geochim. Cosmochim. Acta* **59**, 4147–4165 (1995).

57. Klemm, V., Levasseur, S., Frank, M., Hein, J. R. & Halliday, A. N. Osmium isotope stratigraphy of a marine ferromanganese crust. *Earth Planet. Sci. Lett.* **238**, 42–48 (2005).

58. Klemm, V., Frank, M., Levasseur, S., Halliday, A. N. & Hein, J. R. Seawater osmium isotope evidence for a middle Miocene flood

basalt event in ferromanganese crust records. *Earth Planet. Sci. Lett.* **273**, 175–183 (2008).

59. Sato, H. et al. Rhenium-osmium isotope evidence for the onset of volcanism in the central Panthalassa Ocean during the Norian "chaotic carbon episode". *Glob. Planet. Chang.* **229**, 104239 (2023).
60. Tagle, R. et al. Platinum group elements in impactites of the ICDP Chicxulub drill core Yaxcopoil-1: are there traces of the projectiles? *Meteorit. Planet. Sci.* **39**, 1009–1016 (2004).
61. Collins, G. S. et al. A steeply-inclined trajectory for the Chicxulub impact. *Nat. Commun.* **11**, 1480 (2020).
62. Jones, H. L., Lowery, C. M. & Bralower, T. J. Delayed calcareous nannoplankton boom-bust successions in the earliest Paleocene Chicxulub (Mexico) impact crater. *Geology* **47**, 753–756 (2019).
63. Lowery, C. M. & Bralower, T. J. Elevated post K-Pg export productivity in the Gulf of Mexico and Caribbean. *Paleoceanogr. Paleoclimatol* **37**, e2021PA004400 (2022).
64. Metsana-Oussaid, F., Belhai, D., Arenillas, I., Arz, J. A. & Gilabert, V. New sections of the Cretaceous-Paleogene transition in the southwestern Tethys (Médéa, northern Algeria): planktic foraminiferal biostratigraphy and biochronology. *Arab. J. Geosci.* **12**, 217 (2019).
65. Ishikawa, A., Senda, R., Suzuki, K., Dale, C. W. & Meisel, T. Re-evaluating digestion methods for highly siderophile element and [187]Os isotope analysis: evidence from geological reference materials. *Chem. Geol.* **384**, 27–46 (2014).
66. Birck, J. L., Barman, M. R. & Capmas, F. Re-Os isotopic measurements at the femtomole level in natural samples. *Geostand. Newslett.* **21**, 19–27 (1997).
67. Hay, W. W. et al. Alternative global cretaceous paleogeography evolution of the cretaceous ocean-climate system. *Geol. Soc. Am. Spec. Pap.* **332**, 1–47 (1999).
68. Fischer-Gödde, M., Becker, H. & Wombacher, F. Rhodium, gold and other highly siderophile element abundances in chondritic meteorites. *Geochim. Cosmochim. Acta* **74**, 356–379 (2010).
69. Peucker-Ehrenbrink, B. & Jahn, B.-M. Rhenium-osmium isotope systematics and platinum group element concentrations: Loess and the upper continental crust. *Geochem. Geophys. Geosyst.* **2**, 2001GC000172 (2001).
70. Chen, K. et al. Platinum-group element abundances and Re–Os isotopic systematics of the upper continental crust through time: evidence from glacial diamictites. *Geochim. Cosmochim. Acta* **191**, 1–16 (2016).

Acknowledgements

Author contributions

Competing interests

The authors declare no competing interests.

Additional information

Supplementary information The online version contains supplementary material available at https://doi.org/10.1038/s41467-025-58112-x.

Correspondence and requests for materials should be addressed to Honami Sato.

Peer review information *Nature Communications* thanks Mark Leckie, and the other, anonymous, reviewer(s) for their contribution to the peer review of this work. A peer review file is available.

Reprints and permissions information is available at http://www.nature.com/reprints

Publisher's note Springer Nature remains neutral with regard to jurisdictional claims in published maps and institutional affiliations.